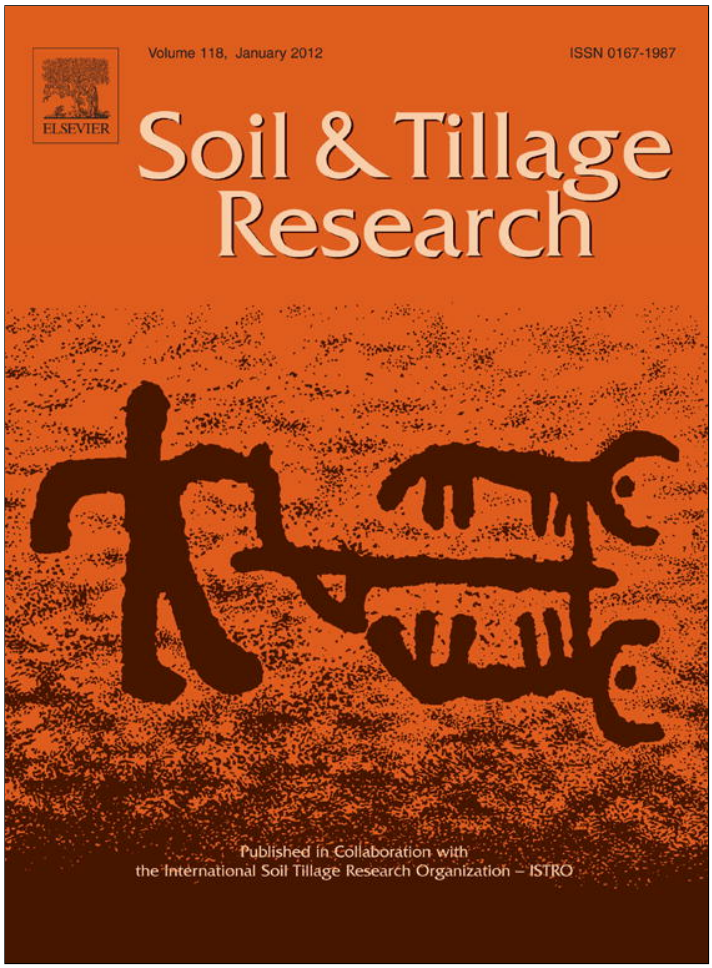

(This is a sample cover image for this issue. The actual cover is not yet available at this time.)

Soil & Tillage Research 122 (2012) 61–66

Contents lists available at SciVerse ScienceDirect

Soil & Tillage Research

journal homepage: www.elsevier.com/locate/still

Microscopy and spectroscopy analysis of carbon nanostructures in highly fertile Amazonian anthrosoils

A. Jorio [a,*], J. Ribeiro-Soares [a], L.G. Cançado [a], N.P.S. Falcão [b], H.F. Dos Santos [c], D.L. Baptista [d], E.H. Martins Ferreira [d], B.S. Archanjo [d], C.A. Achete [d,e]

[a] Departamento de Física, ICEx, Universidade Federal de Minas Gerais, Belo Horizonte, MG 30123-970, Brazil
[b] Departamento de Ciências Agronômicas, Instituto Nacional de Pesquisas da Amazônia, Manaus, AM 69011-970, Brazil
[c] Departamento de Química, ICE, Universidade Federal de Juiz de Fora, Campus Universitário Martelos, Juiz de Fora, MG 36036-330, Brazil
[d] Divisão de Metrologia de Materiais – DIMAT, Instituto Nacional de Metrologia, Normalização e Qualidade Industrial – INMETRO, Xerém, Duque de Caxias, RJ 25250-020, Brazil
[e] Departamento de Engenharia Metalúrgica e de Materiais, Universidade Federal do Rio de Janeiro, Cx. Postal 68505, Rio de Janeiro, RJ 21945-970, Brazil

ARTICLE INFO

Article history:
Received 15 November 2011
Received in revised form 21 February 2012
Accepted 26 February 2012

Keywords:
Amazonian Dark Earth
Soil fertility
Carbon
Electron microscopy
Electron energy loss spectroscpy
Raman spectroscopy

ABSTRACT

The anthropogenic Amazonian soil "Terra Preta de Índio" (Amazonian Dark Earth) provides a potential model for a sustainable land-use system in the humid tropics. A large amount of carbon-based materials in this soil is responsible for its high fertility over long periods of usage, and soil scientists are trying to create "Terra Preta Nova" (New Dark Earth) by adding charcoal as a soil conditioner. By applying materials science tools, including scanning and transmission electron microscopy, energy dispersive X-ray, electron energy loss spectroscopy and Raman spectroscopy, we show that these millenary carbon materials exhibit a complex morphology, with particles ranging in size from micro- to nanometers, from the core to the surface of the carbon grains. From one side, our results might elucidate how nature solved the problem of keeping high levels of ion exchange capacity in these soils. From the other side, morphology and dimensionality are the key issues in nanotechnology, and the structural aspects revealed here may help generating the Terra Preta Nova, effectively improving world agriculture and ecosystem sustainability.

1. Introduction

The humid tropic is home to more than 4 billion people, many of which reside in developing countries. Soils in the humid tropics are characterized by low nutrient retention (Novotny et al., 2009) due to heavy rains and high temperatures. Even in tropical forests such as the Amazonian, the soil is poor and deforestation has led to desertification (Achard et al., 2002). Nevertheless, the pre-Columbian indigenous groups living in the Amazonian forest subsisted on agriculture in addition to hunting, fishing and gathering activities (Simões, 1982). Their way of life generated areas of highly fertile soil rich in plant nutrients known as "Terra Preta de Índio" (Amazonian Dark Earth) (Kern, 1996). This soil is dated up to 7000 years old, and it is generally accepted that they are anthropogenic in origin, although it is not clear whether this was intentional or was a byproduct of human activities (Smith, 1980). "Terra Preta de Índio" is more common in sites at the Amazon basin (Falcão et al., 2003; Glaser et al., 2002; Glaser, 2007; Marris, 2006), but it can also be found throughout the humid tropics and in other regions of South America and Africa (Blackmore et al., 1990; Zech et al., 1990).

The Amazonian Dark Earth sites are 20 ha on average (Glaser, 2007). While the soil in the fertile sites exhibit similar textures and mineralogy to adjacent soils, the key aspect of the fertile sites is the presence of approximately 70 times higher stable carbon content (Glaser et al., 2002). The presence of a large amount of carbon in the "Terra Preta de Índio" is responsible for the stability and recalcitrance of the soil organic matter (Cheng and Lehmann, 2009; Glaser et al., 2001; Liang et al., 2006; Novotny et al., 2009) and for a high soil cation exchange capacity (Liang et al., 2006), which has remained for thousands of years.

Researchers have proposed the production of "Terra Preta Nova" (new Amazonian Dark Earth) by adding charcoal as a soil conditioner to improve the cation exchange capacity, stability and recalcitrance (Glaser et al., 2002; Glaser, 2007; Marris, 2006; Novotny et al., 2009). In addition to the development of a more sustainable agriculture for the humid tropics, this process may increase the C sequestration in soil through a carbon negative release process, which may help prevent desertification. However, charcoal is a disordered, nano-structured carbon that can be produced of various sorts (Marris, 2006). Studies in the field of carbon-related materials have developed different types of well-defined and disordered structures

* Corresponding author. Tel.: +55 31 3409 6610; fax: +55 31 3499 5600.
E-mail address: adojorio@fisica.ufmg.br (A. Jorio).

0167-1987/$ – see front matter © 2012 Elsevier B.V. All rights reserved.
doi:10.1016/j.still.2012.02.009

Table 1
Composition details for the two "Terra Preta de Índio" sites explored in this work.

Sites	pH H_2O	pH KCl	K (Cmolc kg^{-1})	Ca	Mg	Al	t[a]	S[b]	Fe (mg kg^{-1})	Zn	Mn	Cu	P	V[c] (%)	M[d]
Serra Baixa (Iranduba)	5.77	4.43	0.10	3.06	0.51	0.15	3.82	3.67	59.00	15.90	72.90	5.00	214.00	96.07	3.93
Costa Laranjal (Manacapuru)	5.52	5.23	0.17	9.38	1.30	0.05	10.89	10.84	63.20	292.30	843.30	8.00	285.76	99.54	0.46

[a] t: effective cation exchange capacity (sum of K^+, Ca^{2+}, Mg and Al).
[b] S: basis sum (K, Ca and Mg).
[c] V: basis saturation percentage for effective cation exchange capacity.
[d] M: Al saturation percentage for effective cation exchange capacity.

(Boehm, 1994; Dresselhaus, 1998; Noorden, 2011). Here, we study the structure of the carbon materials found in "Terra Preta de Índio" (TPI), which we refer to as TPI-carbons, to elucidate their morphological aspects and the surface science behind their functionality. We show that TPI-carbons exhibit a special nanostructure that might be considered to generate "Terra Preta Nova" (TPN).

2. Materials and methods

The "Terra Preta de Índio" samples used in this work were collected near Manaus, Amazonas State, Brazil, from two sites: Serra Baixa (costa do Açutuba), Iranduba (Lat 3°30′S, Long. 60°20′W) and Costa do Laranjal, Manacapuru (Lat 3°18′33″S, Long. 60°33′21″W). Samples were taken from surface layer (0–20 cm depth) using a Dutch auger. Composition details are shown in Table 1. The charcoal samples were produced in the Charcoal Laboratory at *Instituto Nacional de Pesquisa da Amazônia* (INPA) from different plant species typical of this region: Ingá (*Ingá edulis* Mart.), Embaúba (*Cecropia hololeuca* Miq.), Lacre (*Vismia guianenses* Aubl. Pers) and Bamboo (*Dendrocalamus strictus*). The turf soil was from the Pau Branco mine in the state of Minas Gerais, Brazil.

The TPI soil samples were measured for extractable levels of potassium (K), calcium (Ca), magnesium (Mg), phosphorus (P), iron (Fe), manganese (Mn), copper (Cu), and zinc (Zn) using the Mehlich 1 extraction (HCl 0.05 mol L^{-1} + H_2SO_4 0.0125 mol L^{-1}) (Kuo, 1996), with available P determined colorimetrically using the ammonium molybdate with ascorbic acid method (Braga and Defelipo, 1974). K determined by flame emission photometry, and Ca and Mg determined by atomic absorption spectrophotometry. Exchangeable aluminium with 1 mol L^{-1} KCl titrated with 0.025 mol L^{-1} NaOH. Fe, Mn, Cu and Zn were measured by atomic absorption spectroscopy. The soil pH was determined in water and KCl using an electronic pH meter with a glass electrode. Deionized water and KCl 1.0 mol L^{-1} were applied in the ratio of 1:2.5 soil:solution.

Ingá (*I. edulis* Mart.) biomass came from a 7-year-old tree, Embaúba (*C. hololeuca* Miq.) biomass from a 3-year-old tree, Lacre (*V. guianenses* Aubl. Pers.) biomass from a 4-year-old tree and Bamboo (*D. strictus*) biomass from a 10-year-old tree. Similar diameter woody materials were chosen and placed in the furnace. In the case of Ingá, the branches were used; for Lacre, Embaúba and Bamboo the middle of the tree trunk of the central stem was used, avoiding the base and top. The biochar was made from the fresh material in the pyrolysis furnace. The three combustion temperatures were 600 °C. Carbonization was accomplished in a pyrolysis furnace of refractory brick with a 20l capacity, reaching the temperature after a 2 h period. In sequence, the furnace was turned off and allowed to cool. After combustion, the samples were filtered with a 2 mm sieve.

Scanning electron microscopy (SEM) images were obtained using a Nova Nanolab 600 dual beam platform from FEI, and different samples were analyzed similarly, being acquired on the same equipment using 10 keV accelerating energy and 0.13 nA electron current. Selected grains were cut using a focused ion beam (FIB) in the same equipment, the ion bombardments being performed using a Ga^+ ion source working at 30 keV accelerating energy with an ion current of about 1.6 pA. Thin cross-sections were removed and welded onto a lift-out copper grid for subsequent analyses. As described further, transmission electron microscopy (TEM), scanning transmission electron microscopy (STEM), energy dispersive X-ray (EDX) microscopy and spatially localized electron energy loss spectroscopy (EELS) were performed on a Cs-corrected FEI Titan 80/300 transmission electron microscope, equipped with a Gatan imaging filter Tridiem and an EDX analyzer. The EELS spectra were collected using an electron monochromator, reaching an ultimate energy resolution of 0.2 eV. The spectroscopic techniques (EDX and EELS) were performed in STEM mode, allowing nanometer scale spatial resolution. The elemental mappings were obtained by integrating characteristic X-ray signals during a drift-corrected STEM spectrum imaging experiment. STEM images were acquired using a high-angle annular dark-field detector.

Raman scattering measurements were performed in the TPI-carbons with the following: (1) an Andor™ Tecnology-Sharmrock sr-303i spectrometer, coupled with a charge-coupled device (CCD) detector in the backscattering configuration using a 60× objective lens and a 632.8 nm He–Ne excitation laser and (2) a T64000 Horiba Jobin-Yvon spectrometer coupled with a charge coupled device (CCD) detector in the backscattering configuration using a 50× objective lens and both 514.5 nm and 488.0 nm laser lines from an Ar^+ laser. For statistical analysis, the samples were measured as received, deposited on a cover slip, and after dissolution in DI water, a drop being placed onto an individual cover slip and measured after it dried. Furthermore, a randomly selected TPI-carbon grain was sectioned in a way that the exposed interface was turned to a cover slip, and spatially localized Raman spectra were obtained from the interior (core) and the exterior (surface) regions. The charcoal and turf samples were also characterized with Raman spectroscopy. To fix the samples on a glass cover slip, droplet-sized amounts of samples were deposited on deionized water drops on the cover slip and let dry.

3. Results and discussion

Fig. 1(a) shows a typical scanning electron microscopy (SEM) image of a randomly collected TPI-carbon grain, which measures on a scale of a few 100 μm. Various grain shapes were observed and were generally nonspherical, which is in agreement with a biochar origin (Stoffyn-Egli et al., 1997).

Conventional transmission electron microscopy (TEM) analysis of the TPI-carbon cross-sectioned slices showed two topologically distinct zones (see Fig. 1(b)). One zone demonstrated continuous contrast, was microns in scale, and composed the bulk grain core. The other zone exhibited a submicron porous structure formed by assembling 10–1000 nm particles that were located on the external part of the grain and composed the grain surface. A scanning transmission electron microscopy (STEM) image of a

typical nanometer carbon particle extracted from the external region of the TPI-grain is shown in Fig. 1(c). The particle surface was formed by smaller structures, which were several tens to hundreds of nanometers in length (Fig. 1(c)).

Fig. 1(d) shows an energy dispersive X-ray (EDX) microscopic mapping sequence for the carbon nanoparticle shown in Fig. 1(c). The small carbon particle extracted from the external region of the TPI-grain was rich in O and Ca diffused along the carbonaceous structure, which was observed via oxygen and calcium mapping (see Fig. 1(d)). Phosphorous, chlorine and nitrogen were found in smaller quantities. The particle also contained abundant amounts of Fe, Al, Si, O and P on its border (see three rightmost panels in Fig. 1(d)) along with smaller amounts of chlorine and nitrogen (not shown). These metal oxide-rich nanoparticles were visible on a scale of 10–100 nm. Overall, the elemental maps demonstrated the mechanism by which the porous surface structure helps to adsorb the complementary ingredients that contribute to the high fertility of "Terra Preta de Índio". The nutrient content, which is represented by the abundance of each element, vary largely among grains and among the sites of Amazonian Black Earth, which is in agreement with chemical analysis (Falcão et al., 2003).

Guided by the SEM, spatially localized electron energy loss spectroscopy (EELS) was performed to probe the chemical state of both the core and the external regions of the TPI-carbon grains (Fig. 2(a)) (Batson, 1993; Ma et al., 1993). Well-defined energy peaks were observed in the EELS spectra and demonstrated the presence of ordered structures with signals representing carbon $1s \rightarrow \pi^*$ and $1s \rightarrow \sigma^*$ electronic transitions, which indicate sp^2 hybridization carbon structures. In the $1s \rightarrow \pi^*$ range, four well-defined main peaks were assigned: the aromatic-C peak at 285 eV, the phenol-C peak at 286.7 eV, the aromatic carbonyl peak at 287 eV and the carboxyl peak at 288.6 eV (Lehmann et al., 2005). The relative peak intensities for the spectra shown in Fig. 2(a) indicate that the core is more graphitic than the surface. The external region of the grain demonstrated a deeper level of oxidation, which caused an increase in the abundance of phenol, carbonyl and carboxylic groups.

Resonance Raman spectroscopy is another tool which provides structural information of carbon materials (Cançado et al., 2006, 2007; Ferrari and Robertson, 2000, 2001; Takai et al., 2003). Fig. 2(b) shows the Raman spectra of a TPI-carbon grain, obtained from the grain core (bottom spectrum) and from the grain surface

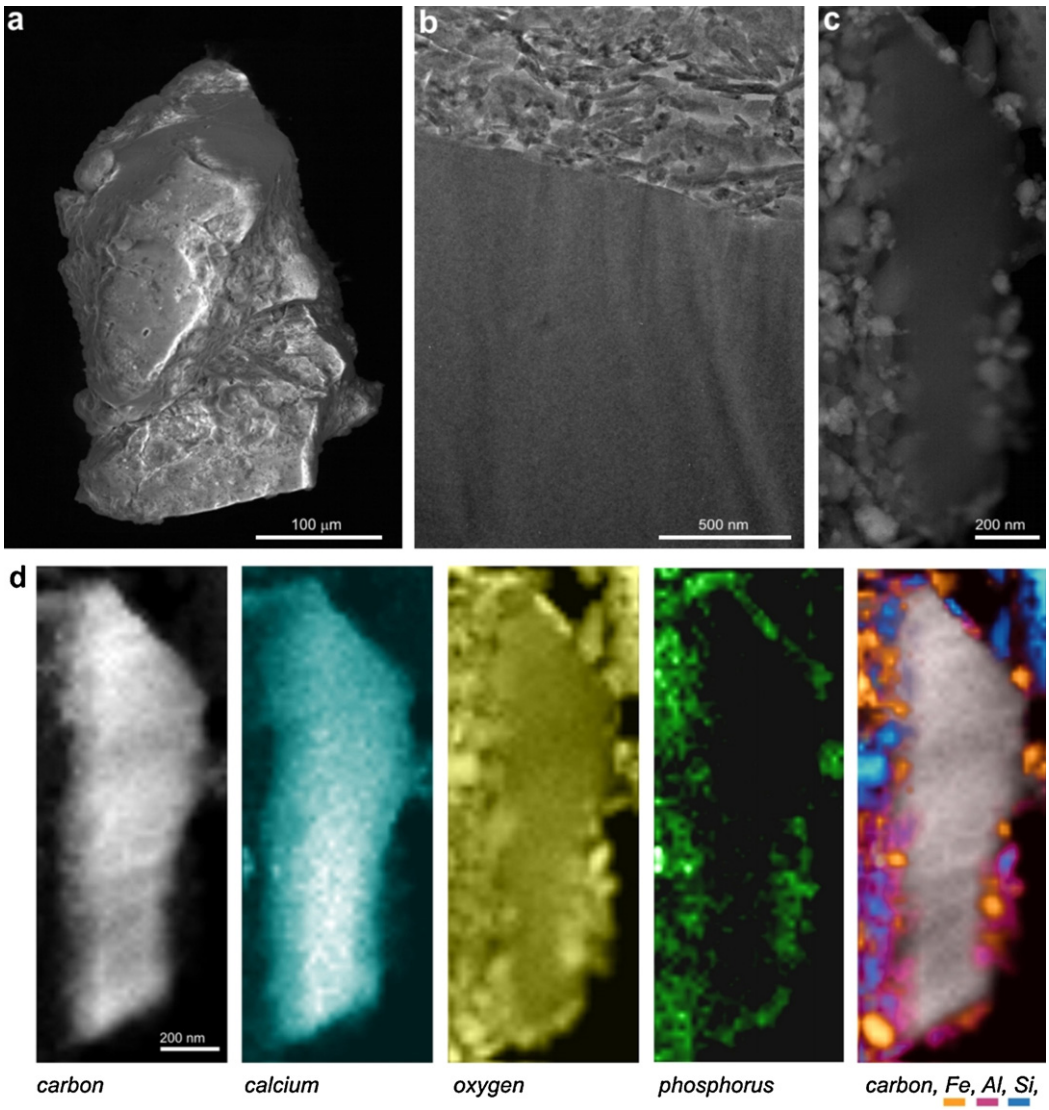

Fig. 1. Microscopy analysis of a TPI-carbon grain. (a) Scanning electron microscopy (SEM) of a commonly observed grain that exhibits a nonspherical shape and is hundreds of nanometers in size; (b) transmission electron microscopy (TEM) of a thin cross-section of the grain showing the interface between the bulk graphitic core and its highly porous nanostructured surface; (c) magnified image using a scanning transmission electron microscope (STEM) of the nanostructured surface of a carbon nanoparticle, which was further analyzed by energy dispersive X-ray (EDX) to determine the local chemical composition (d); the various elements are labeled below each panel.

(top spectrum). The major spectroscopic signature was given by two broad peaks, labeled G and D, at ~1580 cm^{-1} and ~1350 cm^{-1}, respectively. These two features can be related to the presence of D_{6h}-symmetry carbon systems, and the observed G-band frequency and the D to G integrated area ratio are consistent with sp^2 hybridized carbon nanocrystallites (Cançado et al., 2006, 2007; Ferrari and Robertson, 2000, 2001; Lucchese et al., 2010; Takai et al., 2003). The predominance of sp^2 phase in graphitic nanocrystallites is usually indicated by the nondispersive behavior of the D and G peaks in the resonance Raman measurements (Ferrari and Robertson, 2001), which is in agreement with our measurements in the TPI-carbons performed with three excitation laser lines (633 nm, 514 nm and 488 nm). The Raman analysis cannot rule out the presence of well-structured sp^3 carbons, since the resonant contribution from sp^2 carbons overcome the contribution from sp^3 carbons. However, the signal we observe is indeed dominated by the graphitic cores, and the spectral difference from the top to the bottom spectrum in Fig. 2(b) is consistent with the EELS results, as discussed below.

In sp^2 layered carbons, Raman spectroscopy can be used to measure the nanocrystallite dimensions, which are defined by the in-plane crystallite size (L_a) (Cançado et al., 2006, 2007; Ferrari and Robertson, 2000, 2001; Takai et al., 2003). Considering the Raman spectroscopy comes predominantly from the resonant sp^2 carbon, insight about the in-plane dimension L_a of the nanocrystalline structures composing these grains can be obtained from the analysis of the G peak full-width at half maximum (Γ_G) (Cançado et al., 2006, 2007, 2011; Ferrari and Robertson, 2000, 2001; Lucchese et al., 2010; Martins Ferreira et al., 2010; Takai et al., 2003). For example, Γ_G = 108 cm^{-1} and Γ_G = 264 cm^{-1} were found for the bottom (grain core) and top (grain surface) spectra in Fig. 2(b). Considering the $\langle L_a \rangle \propto 1/\Gamma_G$ relation obtained for heat treated diamond-like carbons (Cançado et al., 2007), the average crystallite size $\langle L_a \rangle$ in the core of the carbon grain is $\langle L_a \rangle$ = 5.8 nm, while at the surface $\langle L_a \rangle$ = 2.2 nm. Statistical analysis of the measured Γ_G indicates average crystallite size ranging mostly from $\sim 2 < \langle L_a \rangle < \sim 8$ nm. A total of 60 TPI-carbon grains from two TPI sites were measured. This aspect seems to be important for both the stability of the carbon structure and for improving the cation absorption and release in the graphitic structure (e.g., see Fig. 1(d) for Ca).

The importance of the Γ_G Raman analysis can be demonstrated by comparing results from the TPI-carbons with results from (i) turf (or peat), which is another highly productive black soil formed by the accumulation of partially decayed vegetative matter and (ii) different samples of charcoal from different vegetable sources that are intentionally produced for TPN ("Terra Preta Nova") generation (see spectra in Fig. 3(a)). Fig. 3(b) plots the measured distribution for Γ_G. The charcoal produced for TPN generation did not exhibit

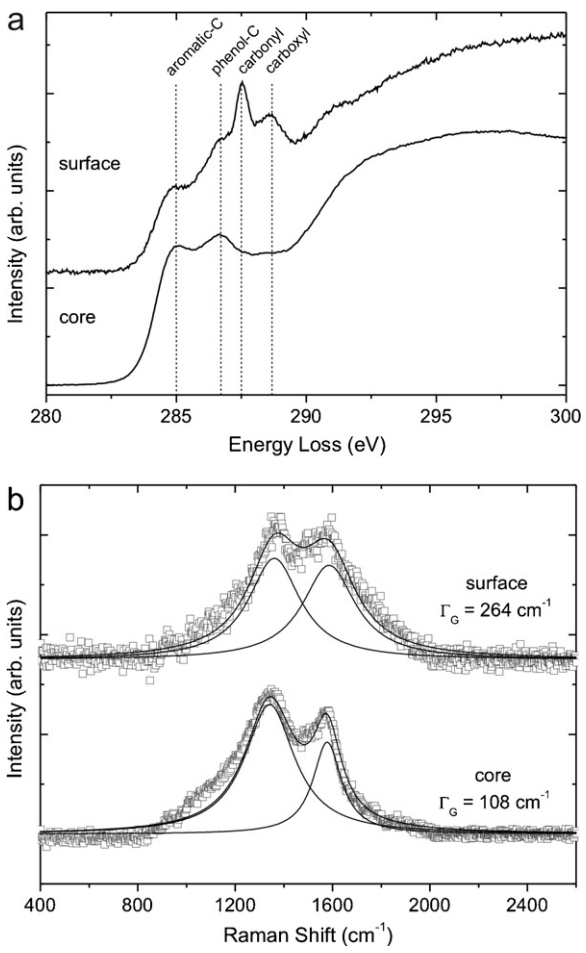

Fig. 2. Spectroscopy analysis of a TPI-carbon grain. (a) Electron energy loss spectra and (b) Raman spectra of the core (bottom spectra) and the surface (top spectra) of two TPI-carbon grains.

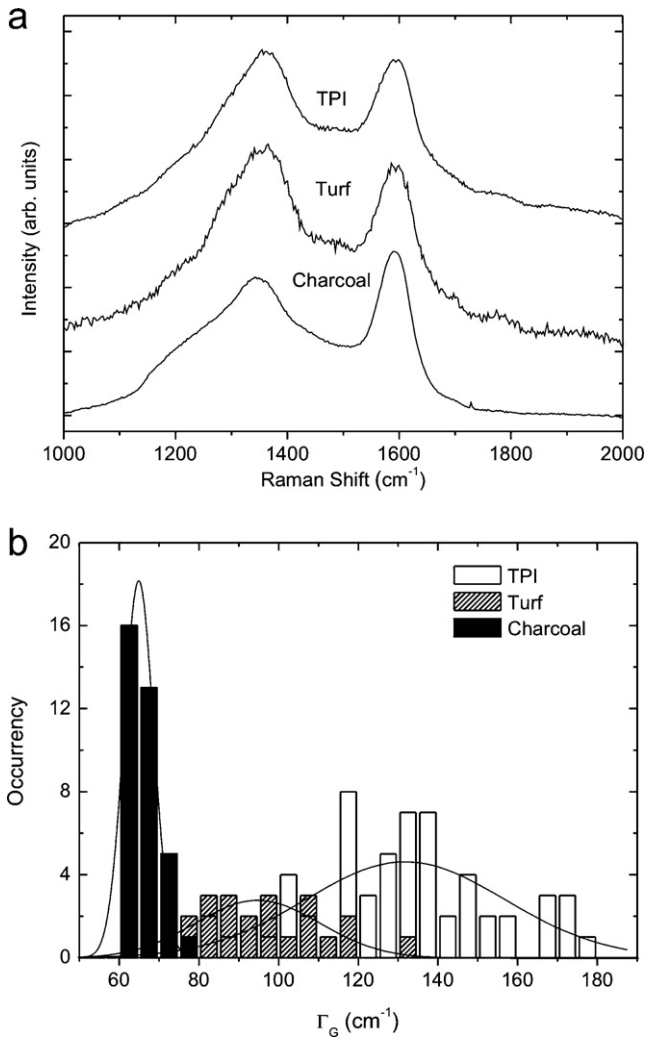

Fig. 3. Statistical Raman spectroscopy analysis for crystallite dimensionality. (a) Raman spectra from TPI-carbon (top), turf (middle) and charcoal (bottom). (b) Statistical analysis of the Γ_G from TPI-carbons, turf and charcoal obtained with a 632.8 nm laser.

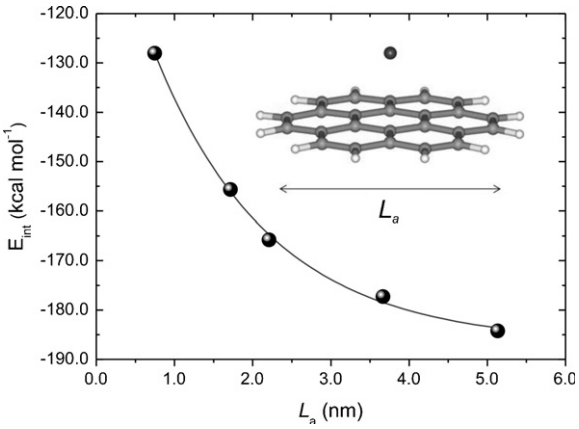

Fig. 4. Quantum chemistry analysis of the graphene–Ca(II) complex stability. The interaction energy is plotted as a function of the graphene plane diameter L_a. The calculations were performed using the PM3 semi-empirical quantum chemistry method (Stewart, 1989; Suzuki et al., 2003).

the expected carbon nanostructure because the Γ_G was too small (i.e. L_a was too large). Considering the $\langle L_a \rangle \propto 1/\Gamma_G$ relation from (Cançado et al., 2007; Takai et al., 2003), the crystallite size distribution for a piece of charcoal was typically found between 8 and 12 nm, while the TPI-carbons were found in the $\langle L_a \rangle \sim 3$–8 nm range.

To gain insights about the importance of the primary grain sizes L_a, theoretical calculations were performed using the PM3 semiempirical quantum chemistry method (Stewart, 1989), which has been shown to be suitable to study large graphene sheets and has been applied to study Li-ion batteries (Suzuki et al., 2003). Several polycyclic hydrocarbon molecules with a general formula C_nH_m ($n = 24$–726; D_{6h} symmetry) were used as modes for graphene sheets. For this series, the diameter (L_a) ranged from 0.7 to 5.1 nm. Fig. 4 plots the L_a dependence of the Ca(II)–graphene complex energy interaction obtained with quantum chemistry calculations (Stewart, 1989; Suzuki et al., 2003). The stability of the Ca(II)–graphene complex decreases and the energy increases for sheets smaller than 3 nm in diameter, while for values larger than 3 nm, the interaction energies converge ($E_{int} \sim -190$ kcal mol^{-1}). However, for in-plane sizes $L_a > 8$ nm, the absorption and release of other elements into the graphitic structure is likely to be naturally reduced. Due to a decrease in the surface-to-volume ratio and interlayer distances (Dresselhaus, 1998), the nanographite particle tends to be an inert structure, similar to bulk graphite. Therefore, the nanosized aspect of the carbon structure seems to be optimum. A critical value of about ~2–8 nm for graphitic crystallites implies an active structure that reconciles functionality with cation absorption stability. Furthermore, it serves as a colloidal mineral that regulates the retention and delivery of nutrients from the soil solution to the root plant system where nutrients are absorbed.

4. Conclusion

To conclude, we have applied the knowledge in the field of carbon materials science to address a complex problem related to soil science. Based in our results, we agree that the carbon phase in "Terra Preta de Índio" started as a charcoal-like structure, as believed by soil scientists. This type of structure is stable and does not leach. In sequence, the environment action over thousands of years might have degraded the surface and, as a result, the in-plane crystallite size (L_a) was diminished towards maximum catalytic functionality, allowing the formation of the unusually highly fertile soils. Fig. 5 shows schematics that illustrate our model for the sectioned TPI-carbon structure.

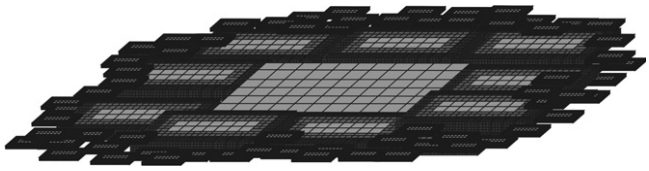

Fig. 5. Schematics showing the crystallite size distribution a sectioned TPI-carbon grain, showing a "fractal-like" structure, with crystallite sizes ranging from $\langle L_a \rangle \sim 5$–8 nm at the core and from $\langle L_a \rangle \sim 2$–5 nm at the surface.

According to Havlin et al. (2005), increasing the number of negative charges on the surface of clay minerals and organic matter increases the cation exchange capacity of soils. Dissociation of H^+ from carboxylic acid and phenolic acid groups generate the negative charges. As the pH increases, some of these H^+ ions were neutralized, which increased the negative surface charge (Havlin et al., 2005). Combining this information with the data presented here, it is clear that the external region of the grains contributes significantly to the high cation exchange capacity of the soil, while the graphitic core structures act as a sink for cations, such as Ca, and also as a reservoir of graphitic structure for millennia of degradation. This type of degradation increases the cation exchange capacity of the soil, its ability to retain nutrients and its fertility. The large amount of organic residues from animal and vegetative origin provides macronutrients (N, P, K, Ca, Mg, and S) and micronutrients (Fe, Zn, Cu, Mn, B, and Mo) retained by the carbon nanoparticles with primary particles in the ~2–8 nm scale. Our analysis is certainly limited when considering the complexity of the problem, but it is clear that the structural aspects of the TPI-carbons are different from those of recently produced charcoal, which is consistent with the fact that the simple addition of charcoal as a soil amendment does not generate an efficient TPN. For TPN generation, agronomists may have to consider the use of amorphous carbon nanostructures with the proprieties reported here.

Acknowledgments

This work was supported by Pró-Reitoria de Pesquisa-UFMG, Inmetro, FINEP, FAPERJ, FAPEMIG, CNPq (Universal Grant, Rede SPM Brasil, INCT-NanoCarbono) and INPA.

References

Achard, F., Eva, H.D., Stibig, H.J., Mayaux, P., Gallego, J., Richards, T., Malingreau, J.P., 2002. Determination of deforestation rates of the world's humid tropical forests. Science 297, 999–1002.

Batson, P.E., 1993. Carbon 1s near-edge-absorption fine structure in graphite. Phys. Rev. B 48, 042608–042610.

Blackmore, A.C., Mentis, M.T., Scholes, R.J., 1990. The origin and extent of nutrient-enriched patches within a nutrient-poor savanna in South Africa. J. Biogeogr. 17, 463–470.

Boehm, H.P., 1994. Some aspects of the surface chemistry of carbon blacks and other carbons. Carbon 32 (5), 759–769.

Braga, J.M., Defelipo, B.V., 1974. Determinação espectrofotométrica de fósforo em extratos de solo e material vegetal. R. Ceres 21, 73–85.

Cançado, L.G., Takai, K., Enoki, T., Endo, M., Kim, Y.A., 2006. General equation for the determination of the crystallite size L_a of nanographite by Raman spectroscopy. Appl. Phys. Lett. 88, 163106.

Cançado, L.G., Jorio, A., Pimenta, M.A., 2007. Measuring the absolute Raman cross section of nanographites as a function of laser energy and crystallite size. Phys. Rev. B 76, 064304.

Cançado, L.G., Jorio, A., Martins Ferreira, E.H., Stavale, F., Achete, C.A., Capaz, R.B., Moutinho, M.V.O., Lombardo, A., Kulmala, T.S., Ferrari, A.C., 2011. Quantifying defects in graphene via Raman spectroscopy at different excitation energies. Nano Lett. 11, 3190–3196.

Cheng, C.H., Lehmann, J., 2009. Ageing of black carbon along a temperature gradient. Chemosphere 75 (8), 1021–1027.

Dresselhaus, M.S., 1998. The wonderful world of carbon. In: Yoshimura, S., Chang, R.P.H. (Eds.), Supercarbon: Synthesis, Properties and Applications. Springer-Verlag, Berlin.

Falcão, N.P.S., Comerford, N., Lehmann, J., 2003. Determining nutrient bioavailability of amazonian dark earth soils – methodological challenges. In: Lehmann, J., Kern, D.C., Glaser, B., Woods, W.I. (Eds.), Amazonian Dark Earths; Origins, Properties, Management. Kluwer Academic Publishers, pp. 255–270.

Ferrari, A.C., Robertson, J., 2000. Interpretation of Raman Spectra of disordered and amorphous carbons. Phys. Rev. B 61 (20), 14095–14107.

Ferrari, A.C., Robertson, J., 2001. Resonant Raman spectroscopy of disordered, amorphous, and diamondlike carbon. Phys. Rev. B 64, 075414.

Glaser, B., Haumaier, L., Guggenberger, B., Zech, W., 2001. The 'Terra Preta' phenomenon: a model for sustainable agriculture in the humid tropics. Naturwissenschaften 88, 37–41.

Glaser, B., Lehmann, J., Zech, W., 2002. Ameliorating physical and chemical properties of highly weathered soils in the tropics with charcoal – a review. Biol. Fertil. Soils 35, 219–230.

Glaser, B., 2007. Prehistorically modified solids of central Amazonia: a model for sustainable agriculture in the twenty-first centure. Philos. Trans. R. Soc. 362, 187–196.

Havlin, J. L, Beaton, J. D., Tisdale, S. L., Nelson, W. L. 2005. Soil Fertility and Nutrient Management: An Introduction to Nutrient Management. 7th ed.Pearson/Prentice Hall, Upper Saddle River, NJ, pp. 1-515.

Kern, D.C., 1996. Geoquímica e Pedogeoquímica em sítios Arqueológicos com terra preta na Floresta Nacional de Caxiuanã. Ph.D. Thesis. Universidade Federal do Pará, Belém Portel-PA, Brazil.

Kuo, S., 1996. Phosphorus. In: Bigham, J.M. (Editor-in-Chief), Methods of Soil Analysis. Part 3. Chemical Methods – SSSA Book Series No. 5. Soil Science Society of America, Madison, WI USA, pp. 869–919.

Lehmann, J., Liang, B., Solomon, D., Lerotic, M., Luizão, F., Kinyangi, J., Schäfer, T., Wirick, S., Jacobsen, C., 2005. Near-edge X-ray absorption fine structure (NEXAFS) spectroscopy for mapping nano-scale distribution of organic carbon forms in soil: application to black carbon particles. Global Biogeochem. Cycles 19, GB1013.

Liang, B., Lehmann, J., Solomon, D., Kinyangi, J., Grossman, J., O'Neill, B., Skjemstad, J.O., Thies, J., Luizão, F.J., Petersen, J., Neves, E.G., 2006. Black carbon increases cation exchange capacity in soils. Soil Sci. Soc. Am. J. 70 (5), 1719–1730.

Lucchese, M.M., Stavale, F., Martins Ferreira, E.H., Vilani, C., Moutinho, M.V.O., Capaz, R.B., Achete, C.A., Jorio, A., 2010. Quantifying ion-induced defects and Raman relaxation length in graphene. Carbon 48 (5), 1592–1597.

Ma, Y., Skytt, P., Wassdahl, N., Glans, P., Mancini, D.C., Guo, J., Nordgren, J., 1993. Core excitons and vibronic coupling in diamond and graphite. Phys. Rev. Lett. 71, 223725–223728.

Marris, E., 2006. Black is the new green. Nature 442, 626–628.

Martins Ferreira, E.H., Moutinho, M.V.O., Stavale, F., Lucchese, M.M., Capaz, R.B., Achete, C.A., Jorio, A., 2010. Evolution of the Raman spectra from single-, few-, and many-layer graphene with increasing disorder. Phys. Rev. B 82, 125429.

Noorden, R.V., 2011. The trials of new carbon. Nature 469, 14–16.

Novotny, E.H., Hayes, M.H.B., Madari, B.E., Bonagamba, T.J., deAzevedo, E.R., de Souza, A.A., Song, G., Nogueira, C.M., Magrich, A.S., 2009. Lessons from the Terra Preta de Índios of the Amazon region for the utilisation of charcoal for soil amendment. J. Braz. Chem. Soc. 20 (6), 1003–1010.

Simões, M.F., 1982. A Pré-História da Bacia Amazônica: Uma tentativa de reconstituição. In: Cultura Indígena, Textos e Catálogo, Semana do Índio, Museu Goeldi, Belém, pp. 5–21.

Smith, N.J.H., 1980. Anthrosols and human carrying capacity in Amazonia. Ann. Assoc. Am. Geogr. 70 (4), 553–566.

Stewart, J.J.P., 1989. Optimization of parameters for semiempirical methods. I. Method. J. Comp. Chem. 10, 209–220.

Stoffyn-Egli, P., Potter, T.M., Leonard, J.D., Pocklington, R., 1997. The identification of black carbon particles with the analytical scanning electron microscope: methods and initial results. Sci. Total Environ. 198, 211–223.

Suzuki, T., Hasegawa, T., Mukai, S.R., Tamon, H., 2003. A theoretical study on storage states of Li ions in carbon anodes of Li ion batteries using molecular orbital calculations. Carbon 41, 1933–1939.

Takai, K., Oga, M., Sato, H., Enoki, T., Ohki, Y., Taomoto, A., Suenaga, K., Iijima, S., 2003. Structure and electronic properties of a nongraphitic disordered carbon system and its heat-treatment effects. Phys. Rev. B 67, 214202.

Zech, W., Haumaier, L., Hempfling, R., 1990. Ecological aspects of soil organic matter in tropical land use. In: McCarthy, P., Clapp, C.E., Malcolm, R.L., Bloom, P.R. (Eds.), Humic Substances in Soil and Crop Sciences: Selected Readings. American Society of Agronomy and Soil Science Society of America, Madison, WI, USA, pp. 187–202.